TECHNICAL MEMORANDUM

538

A Reduced Radiation Grid for the ECMWF Integrated Forecasting System

Jean-Jacques Morcrette, George Mozdzynski and Martin Leutbecher

Research Department

ECMWF, Shinfield Park, Reading
RG2 9AX, United Kingdom

Jean-Jacques.Morcrette@ecmwf.int

September 21, 2007

European Centre for Medium-Range Weather Forecasts
Europäisches Zentrum für mittelfristige Wettervorhersage
Centre européen pour les prévisions météorologiques à moyen terme

Abstract

A specific interface between the radiation transfer calculations and the rest of the ECMWF model was introduced in 2003, potentially providing substantial economy in computer time by reducing the spatial resolution at which radiation transfer is evaluated, without incurring some of the deficiencies produced by the sampling strategy previously used in the ECMWF model. The introduction of a new radiation package (McRad) in June 2007 has led to a more extensive use of this interface, and its impact is discussed in this note.

For a given model resolution, the impact of a lower resolution radiation grid on the model behaviour is studied here, in the context of 10-day forecasts at high resolution ($T_L799L91$), of medium resolution forecasts ($T_L399L62$) used in the Ensemble Prediction System (EPS), and of low resolution simulations ($T_L159L91$) as used for model development and seasonal forecasts with an interactive mixed-layer ocean.

Results for the high resolution forecasts are compared in terms of objective scores and of the quality of "surface" parameters (total cloud cover, two-metre temperature and specific humidity, and 10-m wind) usually verified in a meteorological context. For the medium resolution forecasts, the impact of the radiation grid is studied in terms of the potential increase in the efficiency of the EPS system without deteriorating the probabilistic skill. Impact of changes in the radiation grid resolution on the low resolution versions of model is discussed in terms of cloud-radiation interactions and ocean surface temperature.

1. Introduction

In atmospheric general circulation models, the representation of the radiation transfer within the atmosphere is usually the most expensive among the various parametrisations of the physical processes. If the impact of the radiation transfer were to be computed for every grid point and at all time steps, it would generally require as much CPU time or more than the rest of the model dynamical and other physical parametrisations. Traditionally, to limit this radiation burden, radiation transfer is only computed every few model hours. For example, with full radiation computations performed every 2 hours at all grid points, radiation transfer accounts for 27 percent of the run time of the GME forecast model (Majewski et al., 2002).

In the European Centre for Medium-Range Weather Forecasts (ECMWF) $T_L 511 L 60$ model operational till October 2003, radiation transfer represented about 10 percent of the computer time, but was evaluated only every 3 hours on a spatial grid sampled down to 1 point out of 4 in the sub-tropical and tropical areas (Morcrette, 2000).

With the continuous increase in both horizontal and vertical resolutions, the time step is simultaneously reduced (to $\Delta t = 12$ mn for the $T_L 799 L 91$ model operational since February 2006) so the radiation parametrisations, now being called every hour, saw their fractional cost decreasing (7.3 percent of the total computer time for the above configuration), but this limited cost was obtained through the use of a radiation grid twice as coarse as the grid for the rest of the model.

The recent introduction of the McRad package for radiation computations (Morcrette et al., 2007) in the IFS required revisiting the use of this interface for the various meteorological applications run at ECMWF. This flexible interface allows for delocalized radiative computations with potential increase in the computer efficiency of the model through a spatial representation of the radiation transfer differing from that of the other physical processes. Section 2 describes the strategy used and the resulting interface between the radiative parametrisations and the rest of the model is described in more details in an Appendix. Then the impact of this new interface is discussed for different configurations of the model, including medium-resolution forecasts as used in the Ensemble Prediction System in Section 3, high-resolution ten-day forecasts in Section 4, and seasonal simulations at low resolution without and with a coupled ocean model in Sections 5 and 6. Conclusions are given in Section 7.

2. A reduced grid for radiation computations

At ECMWF, the interface for radiation computations in the Integrated Forecasting System (IFS) has evolved over the years to accommodate changes in computer architecture. A description of this evolution including technical details is given in the Appendix.

Prior to the mid-90's, full radiation computations were done every 3 hours for all latitude lines with a horizontal sampling one point out of four in the longitudinal direction. On this sampled radiation grid, a shortwave (SW) transmissivity was computed at the layer interface by dividing the net SW flux by μ, the cosine of the solar zenith angle at the mid-point of the time interval between two full radiation calculations. These full radiation quantities were then interpolated back to the normal physical grid. The net longwave fluxes were kept fixed between two full radiation time steps whereas the net SW fluxes were evaluated at every time step. For every time step within the period between two full radiation computations, the net SW fluxes were obtained by multiplying the SW transmissivity by μ relevant for the time step and grid point. This approximate treatment therefore was making the radiation fields interact with cloudiness only every 3 hours, and further was introducing spatial smoothing of the cloud-radiation interactions.

From September 1991, the ECMWF model started to use a reduced horizontal grid for all its computations,

keeping roughly the same grid size (in km) when going from Equator to poles (Hortal and Simmons, 1991). On input, model fields required by the radiation package were still sampled on each latitude with one point out of four being selected in sub-tropical and tropical areas. To accommodate this radiation grid the previous frequency of one in four reduced gradually to every point in polar areas. On output, lagrangian cubic interpolation was used.

A new interface for radiation computations was developed and implemented in October 2003. Radiation calculations are performed on a grid with a coarser resolution than the current model grid. Interpolation between model and radiation grids are performed using interfaces existing within the IFS libraries and as a result help reduce code maintenance.

This radiation grid has been used since October 2003, with a coarsening factor of two in both latitude and longitude w.r.t. the rest of the model (e.g., the operational forecast model at T_L799 after February 2006 was run with a radiation grid $R399$). The operational implementation in June 2007 of a new more computer-intensive radiation package (McRad, Morcrette et al., 2007) with an increased number of spectral intervals in all the ECMWF forecasts applications has led to the search for an optimal radiation grid for the different weather forecasting applications run at ECMWF.

Configuration	Dyn	Rad	Freq	%Rad	Ratio
$T_L799L91$					
CY31R2	799	399	1	7.3	1.000
McRad	799	511	1	36.4	1.456
	799	399	1	26.5	1.262
	799	319(*)	1	19.2	1.147
	799	255	1	13.8	1.076
	799	159	1	6.7	0.994
	799	95	1	3.4	0.960
$T_L399L62$					
CY31R2	399	159	3	4.1	1.000
McRad	399	255	3	31.6	1.403
	399	159	3	16.4	1.148
	399	95(*)	3	7.7	1.039
	399	63	3	3.8	0.998
	399	47	3	3.0	0.989
	399	31	3	2.1	0.980
$T_L159L91$					
CY31R2	159	63	3	8.0	1.000
McRad	159	159	3	67.5	2.831
	159	95	3	45.1	1.675
	159	63(*)	3	27.7	1.273
	159	47	3	19.5	1.143
	159	31	3	11.0	1.034

Table 1: Impact of the McRad radiation package on the timing of the ECMWF model forecasts for different configurations and different horizontal resolutions. *Dyn* is the resolution for the dynamics, *Rad* that for the radiation. *Freq* is the frequency (hour) for calling the full radiation scheme, *%Rad* is the fraction of computer time taken by the radiative transfer calculations. *Ratio* is the factor by which McRad increases the computer cost relative to the previous operational configuration (CY31R2). (*) refers to the operational configuration implemented on 5 June 2007.

Table 1 presents for the various model configurations used at ECMWF an overview of the timing with and without McRad. Depending on the model resolution, associated time-step, and the frequency for calling the full radiation schemes, the cost of the model integration increased from 15 to 29 percent with the adoption of McRad. Comparisons of results with the different radiation grids (from R399 to R95 for the $T_L799L91$ high-resolution model, from R255 to R31 for the $T_L399L62$ model run in the Ensemble Prediction System, from R159 to R31 for the $T_L159L91$ model used for seasonal forecasts, were systematically carried out.

For the choice of the radiation grid, a compromise has to be made between the computer time required to run a given configuration and how detailed one wants the representation of the spatial cloud structure and of its associated radiative fluxes to be. Different meteorological applications lead to different answers: For the high-resolution deterministic forecast where the position of clouds as affected by land-sea temperature and orographic effects is an important factor, the highest radiation resolution is to be kept as much as possible. However, it must be kept in mind that McICA as such allows sub-grid scale information on the horizontal distribution of cloud elements to be taken into account (via the normalized standard deviation), so what appears as a reduced radiation grid in fact includes more information than the original radiation grid used with the pre-McRad scheme. For EPS, the constraint to have the highest radiation resolution possible can certainly be relaxed (see section 3). A best compromise was chosen (R319 for T_L799, R95 for T_L399, R63 for T_L159), which allows the maximum benefit of McRad within the time constraints for delivering the various operational products. The coarsening of the radiation grid was shown to have very little impact on the objective scores provided by high-resolution models, and is further documented in section 4.

The impact, if any, of the reduction in the resolution of the radiation calculations allowed by this flexible radiation grid for other meteorological applications is described in sections 5 and 6.

3. Impact on medium resolution 10-day forecasts as used in the EPS

As discussed in Buizza et al. (1999), for each of the 50 forecast members of the EPS, the model uncertainties deriving from parametrized physical processes are simulated by applying a random number between 0.5 and 1.5 to the sum of the physical tendencies within a $10^o x 10^o$ degree box over three hours. The scaled physical tendencies are then passed to the thermodynamic equation to be solved. Therefore, introducing a more approximate treatment of the radiation tendencies (as through the use of a more reduced radiation grid) is not likely to deteriorate the quality of the EPS forecasts. Table 1 shows the various radiation resolutions from R255 down to R31 that could be used for the current $T_L399L62$ EPS configuration.

In ten-day forecasts with McRad running the $T_L399L62$ model with various resolutions for the radiation grid, the impact on the objective scores was small. For example, Figure 1 presents the r.m.s. error of the temperature at 850 and 200 hPa (the most sensitive parameter) in the Tropics for sets of 93 forecasts starting every fourth day spanning a year from 20060202 to 20070205. For these sets of forecasts with the resolution of the radiation grid being reduced from R255 to R31, the impact on the geopotential is small and does not appear before day 6 of the forecasts (not shown). Similarly small is the impact on the r.m.s. error of temperature at 850 and 200 hPa. Only the mean error in temperature at 850 hPa for all areas (Northern and Southern hemispheres, tropical area) and the mean error in temperature at 200 hPa in the Tropics show a distinct signal. However, the difference between R255 and R31 (i.e, a radiation grid coarsening from $[0.70^o]^2$ to $[5.625^o]^2$) is at most 0.06 K, with the resolutions between R255 and R63 very close to each other, and R47 and R31 showing a more undesirable impact. In the tropics, where these differences in temperature between the various radiation grids are the most marked, the impact on the wind is very small (not shown). So it appears that reducing the resolution of the radiation grid could allow for a decreased cost of the EPS with a rather small effect on its overall quality. Further tests were conducted within the VarEPS (variable resolution EPS) system (Buizza et Al., 2007) running for ten days at T_L399, then at T_L255 for the last five days using three sets of radiation grids:

R159/R95, R95/R63, R47/R31 respectively. Ensemble forecasts were started every other day between 3 Dec 2006 and 2 Jan 2007 (16 cases). As shown in Fig. 2, R47/R31 indeed produces an obvious deterioration of the ranked probability skill score of the temperature at 850 hPa in the Southern hemisphere. The EPS, operational since 5 June 2007, is therefore run at $T_L399L62R95$ then at $T_L255L62R63$.

Rad. Grid	FC+12h Bias (SD) [MAE]			FC+24h Bias (SD) [MAE]			FC+108h Bias (SD) [MAE]			FC+120h Bias (SD) [MAE]		
TCC												
R511	0.45	(2.69)	[1.64]	-0.27	(2.25)	[1.45]	0.25	(3.20)	[2.09]	-0.43	(2.98)	[2.00]
R399	0.45	(2.68)	[1.63]	-0.27	(2.25)	[1.46]	0.26	(3.23)	[2.12]	-0.42	(2.98)	[2.07]
R319	0.46	(2.69)	[1.64]	-0.27	(2.25)	[1.45]	0.24	(3.21)	[2.09]	-0.42	(2.95)	[2.04]
R255	0.44	(2.68)	[1.63]	-0.27	(2.25)	[1.46]	0.27	(3.20)	[2.10]	-0.36	(2.96)	[2.04]
R159	0.45	(2.69)	[1.64]	-0.28	(2.25)	[1.45]	0.27	(3.21)	[2.10]	-0.34	(2.96)	[2.04]
R95	0.44	(2.68)	[1.63]	-0.28	(2.27)	[1.47]	0.23	(3.29)	[2.17]	-0.41	(3.01)	[2.09]
T2m												
R511	-0.05	(2.37)	[1.58]	0.32	(2.13)	[1.41]	-0.02	(3.24)	[2.26]	0.32	(2.90)	[1.97]
R399	-0.06	(2.38)	[1.59]	0.32	(2.12)	[1.40]	-0.02	(3.22)	[2.25]	0.32	(2.89)	[1.96]
R319	-0.07	(2.41)	[1.60]	0.32	(2.13)	[1.41]	-0.04	(3.26)	[2.28]	0.31	(2.91)	[1.97]
R255	-0.07	(2.41)	[1.60]	0.31	(2.14)	[1.41]	-0.06	(3.27)	[2.28]	0.29	(2.91)	[1.98]
R159	-0.09	(2.44)	[1.63]	0.29	(2.13)	[1.41]	-0.08	(3.31)	[2.32]	0.26	(2.90)	[1.97]
R95	-0.07	(2.48)	[1.64]	0.31	(2.18)	[1.43]	-0.05	(3.36)	[2.34]	0.27	(2.95)	[1.99]
Q2m												
R511	-0.04	(0.58)	[0.40]	0.02	(0.64)	[0.45]	-0.02	(0.83)	[0.61]	-0.02	(0.91)	[0.67]
R399	-0.04	(0.58)	[0.40]	0.02	(0.64)	[0.45]	-0.02	(0.83)	[0.61]	-0.01	(0.91)	[0.67]
R319	-0.04	(0.58)	[0.40]	0.02	(0.65)	[0.45]	-0.03	(0.84)	[0.62]	-0.01	(0.91)	[0.67]
R255	-0.05	(0.58)	[0.40]	0.02	(0.65)	[0.45]	-0.03	(0.84)	[0.62]	-0.01	(0.90)	[0.67]
R159	-0.05	(0.59)	[0.40]	0.02	(0.65)	[0.45]	-0.04	(0.84)	[0.62]	-0.02	(0.91)	[0.68]
R95	-0.06	(0.59)	[0.41]	0.03	(0.65)	[0.45]	-0.04	(0.85)	[0.63]	-0.01	(0.92)	[0.69]
W10m												
R511	0.76	(2.17)	[1.76]	0.69	(2.21)	[1.77]	0.64	(2.53)	[2.00]	0.76	(2.80)	[2.23]
R399	0.76	(2.17)	[1.76]	0.69	(2.21)	[1.77]	0.64	(2.54)	[2.00]	0.77	(2.81)	[2.24]
R319	0.76	(2.17)	[1.76]	0.69	(2.21)	[1.78]	0.64	(2.53)	[2.00]	0.77	(2.82)	[2.25]
R255	0.76	(2.17)	[1.76]	0.69	(2.21)	[1.78]	0.65	(2.54)	[2.01]	0.77	(2.82)	[2.25]
R159	0.77	(2.18)	[1.76]	0.69	(2.22)	[1.78]	0.65	(2.56)	[2.02]	0.77	(2.82)	[2.25]
R95	0.77	(2.18)	[1.77]	0.68	(2.21)	[1.78]	0.63	(2.54)	[2.00]	0.75	(2.82)	[2.22]

Table 2: Comparison of surface parameters with values at the synoptic stations over Europe. Results are for sets of T_L799 L91 10-day forecasts for January 2007, with a radiation grid varying from $R511$ to $R95$. *TCC* is the total cloud cover (in oktas), *T2m* is the two-metre temperature (in *K*), *Q2m* is the two-metre specific humidity (in $g\ kg^{-1}$), and *W10m* is the 10-metre wind (in $m\ s^{-1}$).

4. Impact on high-resolution $T_L799L91$ 10-day forecasts

Results in terms of objective scores (anomaly correlation at different geopotential heights, root-mean square and mean errors in temperature and winds) when the radiation resolution is reduced, are not shown for the T_L799 L91 forecasts as they are as or more consistent than for the model at T_L399 L62 discussed in the previous section. Here the emphasis is put on the impact on the so-called surface parameters, the model parameters

that can be verified against measurements at synoptic stations. Table 2 presents the statistics (bias, standard deviation (*SD*) and mean absolute error [*MAE*]) computed for sets of 31 forecasts for January 2007 for a model with a radiation grid varying between $R511$ and $R95$. Table 2 shows that for these parameters, the impact of a reduction of the radiation grid is very small at the beginning of the forecasts, when the model behaviour is largely led by the initial conditions and get slightly larger during the forecasts. However, even at day 5 (FC+108h and FC+120h), the variations in the statistics introduced by the reduction in the radiation grid are small showing that the overall circulation patterns and the three-dimensional distribution of the radiative heating have not had sufficient time to diverge much.

	Annual	DJF	JJA
OLR	-250	-247	-253
R159	-3.99 (9.12)	-2.15 (10.4)	-0.98 (11.8)
R95	-3.93 (9.11)	-2.04 (10.6)	-1.17 (11.6)
R63	-4.07 (8.86)	-2.25 (9.88)	-1.16 (11.0)
R47	-3.89 (8.50)	-1.97 (9.99)	-0.92 (11.2)
R31	-3.74 (8.42)	-1.82 (11.0)	-0.81 (11.2)
ASW	280	288	238
R159	-8.09 (15.9)	-14.4 (22.4)	-7.09 (18.5)
R95	-7.41 (15.4)	-13.7 (21.9)	-6.70 (18.4)
R63	-7.47 (15.4)	-13.5 (21.6)	-6.70 (18.3)
R47	-7.57 (15.1)	-13.5 (21.2)	-7.07 (18.4)
R31	-7.88 (15.8)	-13.7 (22.3)	-7.49 (18.9)
LWCF	28.5	29.1	27.3
R159	-5.43 (9.31)	-6.51 (11.2)	-4.23 (10.8)
R95	-5.37 (9.26)	-6.50 (11.4)	-4.22 (10.6)
R63	-5.40 (9.10)	-6.45 (10.9)	-4.19 (10.2)
R47	-5.33 (8.90)	-6.44 (11.0)	-4.01 (10.3)
R31	-5.33 (8.83)	-6.43 (11.4)	-4.02 (10.3)
SWCF	-48.7	-51.8	-45.1
R159	-3.28 (14.7)	-3.24 (17.7)	-3.69 (17.5)
R95	-2.69 (14.4)	-2.64 (17.6)	-3.38 (17.5)
R63	-2.77 (14.3)	-2.52 (17.4)	-3.39 (17.2)
R47	-2.90 (14.2)	-2.44 (16.9)	-3.82 (17.5)
R31	-3.15 (14.4)	-2.68 (18.0)	-4.11 (17.7)

Table 3: Annual mean results from sets of 13-month simulations at $T_L159L91$ with different radiation grids. The radiative fluxes at the top-of-the-atmosphere (TOA) (outgoing long-wave radiation OLR, absorbed short-wave radiation ASW, long-wave cloud forcing LWCF and short-wave cloud forcing SWCF in $W\ m^{-2}$) are compared to equivalent CERES measurements. All means, biases and r.m.s. refer to averages over the $50^oN - 50^oS$ latitude band.

	Annual	DJF	JJA
TCWV	29.0	27.7	29.3
R159	-2.20 (3.55)	-2.24 (3.95)	-1.80 (3.69)
R95	-2.05 (3.43)	-2.11 (3.88)	-1.62 (3.54)
R63	-1.99 (3.33)	-2.13 (3.81)	-1.59 (3.47)
R47	-1.91 (3.25)	-2.06 (3.75)	-1.46 (3.43)
R31	-1.85 (3.18)	-1.96 (3.81)	-1.45 (3.48)
TCC	62.2	62.9	61.4
R159	-2.52 (9.62)	-1.30 (10.2)	-1.81 (12.1)
R95	-1.86 (9.72)	-1.30 (10.3)	-1.61 (12.2)
R63	-1.91 (9.83)	-1.19 (10.4)	-1.72 (12.4)
R47	-1.87 (9.62)	-1.14 (9.96)	-1.65 (12.5)
R31	-1.89 (9.90)	-1.07 (11.3)	-1.70 (12.3)
TCLW	84.5	82.5	86.6
R159	-16.5 (25.5)	-13.1 (33.3)	-20.1 (35.8)
R95	-16.4 (25.9)	-14.0 (33.4)	-19.2 (35.3)
R63	-16.0 (25.8)	-13.3 (33.9)	-19.7 (35.4)
R47	-15.9 (25.8)	-13.8 (33.9)	-19.0 (34.8)
R31	-15.7 (25.7)	-13.3 (34.0)	-18.7 (36.0)

Table 4: As in Table 3, but for the total cloud cover (TCC) compared to ISCCP D2 data, and the total column water vapour (TCWV, in $kg\ m^{-2}$) and total column liquid water (TCLW, in $g\ m^{-2}$) compared to SSM/I data.

	Annual	DJF	JJA
TP	2.61	2.58	2.63
R159	0.370 (1.18)	0.347 (1.54)	0.355 (1.65)
R95	0.364 (1.17)	0.359 (1.59)	0.357 (1.65)
R63	0.372 (1.15)	0.356 (1.55)	0.364 (1.62)
R47	0.372 (1.16)	0.343 (1.57)	0.371 (1.64)
R31	0.371 (1.17)	0.347 (1.63)	0.365 (1.73)
T2m ERA40	288	286	290
R159	-0.130 (1.12)	-0.046 (2.05)	-0.306 (0.98)
R95	-0.102 (1.05)	-0.054 (2.10)	-0.216 (0.96)
R63	-0.088 (0.96)	-0.013 (1.82)	-0.164 (1.00)
R47	-0.076 (0.95)	-0.062 (1.77)	-0.135 (0.96)
R31	-0.034 (1.05)	-0.019 (2.01)	-0.085 (1.03)
DT2m ERA40	283	281	285
R159	-0.764 (1.68)	-0.564 (2.46)	-1.065 (1.90)
R95	-0.738 (1.65)	-0.566 (2.52)	-0.989 (1.80)
R63	-0.726 (1.59)	-0.575 (2.28)	-0.914 (1.81)
R47	-0.714 (1.56)	-0.599 (2.19)	-0.900 (1.80)
R31	-0.660 (1.61)	-0.531 (2.45)	-0.825 (1.75)

Table 5: As in Table 3, but for the total precipitation TP (in $mm\ day^{-1}$) compared to GPCP data and temperature T2m (in K) and dew point temperature DT2m (in K) compared to ERA40.

	Annual	DJF	JJA		Annual	DJF	JJA
SSR ocn	155.2	163.7	143.7	STR ocn	-51.8	-52.5	-50.4
R159	13.8	19.8	5.9	R159	-3.1	-2.4	-2.4
R95	14.5	20.8	6.1	R95	-3.5	-2.9	-2.7
R63	14.3	20.6	6.1	R63	-3.4	-2.8	-2.7
R47	14.0	20.5	5.3	R47	-3.1	-2.7	-2.4
R31	13.6	19.9	5.0	R31	-2.9	-2.2	-2.2
SSH ocn	-11.0	-13.7	-9.0	SLH ocn	-96.5	-100.2	-94.2
R159	-2.9	-1.2	-4.2	R159	-6.7	-4.1	-6.6
R95	-2.7	-1.2	-4.1	R95	-6.2	-4.4	-6.5
R63	-2.7	-1.1	-4.1	R63	-6.2	-3.8	-6.4
R47	-2.7	-1.1	-4.2	R47	-6.1	-3.4	-6.5
R31	-2.5	-1.0	-3.8	R31	-5.9	-3.4	-6.0
			Annual	DJF	JJA		
		SNET ocn	-2.2	-0.9	-7.9		
		R159	-0.8	10.2	-9.4		
		R95	0.0	10.3	-9.2		
		R63	-0.0	10.9	-9.2		
		R47	0.0	11.3	-9.9		
		R31	0.2	11.2	-9.2		

Table 6: As in Table 3, but for the ocean surface fluxes (all in $W\ m^{-2}$) compared to the Da Silva-Levitus climatology.

5. Impact on seasonal simulations at $T_L 159 L 91$ with specified SSTs

Sets of 13-month simulations at $T_L 159 L 91$ starting 30 hours apart from 20000801_00UTC to 20000804_18UTC were run with the sea surface temperature updated every day, and with the radiation grid varying from R159 to R31 (see Table 1). The difference to ERA40 of the zonally averaged temperature (Figure 3), zonal wind (Figure 4) and vertical velocity (Figure 5) shows that a large reduction in the radiation grid resolution does not affect markedly the annual mean climate. This is confirmed by the differences in global averaged radiative fluxes, where the annual, winter and summer differences to CERES radiative fluxes at the top of the atmosphere are presented in Table 3. The differences to observations vary by less than 0.4 Wm^{-2} for the outgoing longwave radiation, less than 0.8 Wm^{-2} for the absorbed shortwave radiation, and less than 0.3 and 0.8 Wm^{-2} for the long-wave and short-wave cloud forcing. The differences to observations of the total column water vapour, total cloudiness, total cloud liquid water (Table 4) and total precipitation , two-metre temperature and dew-point temperature (Table 5) remain very similar when going from R159 to R31. As seen in Table 6, the components of the surface energy budget over the ocean show only a small dependence on the resolution of the radiation grid, also seen on the maps of the difference of the surface net heat flux with the Da Silva and Levitus's (1994) climatology (Fig. 6).

6. Impact on seasonal simulations at $T_L 159 L 62$ with an ocean mixed-layer model

Sets of two-year simulations were also run with the $T_L 159$ L62 atmospheric model coupled to a mixed-layer ocean model (Vialard et al., 2005). The ocean model has a horizontal resolution of 2° x 2°, and 20 levels in the vertical. The coupled model was run with the R159, R63 and R31 radiation grids. Figure 7 presents the

differences with ERA-40 (Uppala et al., 2005) of the sea surface temperature (SST) averaged over the first and second year. For the radiation resolution varying from $[1.125^o]^2$ to $[2.8125^o]^2$ to $[5.625^o]^2$, the impact on the SST is small, as the error patterns are very similar from one radiation resolution to the other. From the first year, the Southern ocean is too warm by up to 2 K, with too high SSTs also appearing in the tropics, whereas the mid-latitudes of the Northern hemisphere displays too cold SSTs between 0.3 and 1.5 K. In the second year, the areas with too warm SSTs shrink and concern only the Southern Ocean south of 60^oS and limited areas along the equator. However, these signals are consistent whatever the radiation resolution, corroborating the results found for the model with specified SSTs in section 5. A radiation grid of R63 appears adequate for the operational application, given that, in that case, the coupled model is used within an ensemble prediction system to provide seasonal (up to 9 months) forecasts.

7. Summary and conclusions

Radiation transfer is usually one of the most expensive parametrisations in the numerical atmospheric model. At ECMWF, over the years with changing computer environments, various strategies have been used to keep the fraction of the computation time devoted to radiation transfer under control. The cost of the radiation computations depends on the horizontal and vertical resolutions of the model. It also depends on the frequency at which full radiation computations are carried out, with intermediate time-steps receiving radiation tendencies derived from temporally interpolated fluxes.

For a given model horizontal resolution, an increase in model vertical resolution leads to a reduced time step. As full radiation computations are called with a given frequency independent of the time step, the relative cost of the radiation transfer will therefore decrease compared to the total cost of a model integration with an increase in the model vertical resolution.

Still over the last ten years, full radiation computations have only been performed every three hours (every hour during the first 12 hours) and on a reduced spatial grid (Morcrette, 2000). A neural network approach to the long-wave radiation transfer was also tested in the ECMWF model (Chevallier et al., 2000) and was found to give adequate results (sufficient accuracy together with a six-fold decrease in the computer time for the long-wave radiative calculations) at low to medium vertical resolution (up to 50 layers). At 60 layers and above (the vertical resolution since December 2001), both accuracy and rapidity could not be kept at once given the increased non-linearity in the lowest and uppermost atmospheric layers. Consequently the neural network approach is used only for the 4D-Var linearised physics (Janiskova et al., 2002) when the accuracy requirements are weaker.

This paper has looked at another approach where radiation transfer, thanks to a very flexible interface, can be computed at a lower spatial resolution than the rest of the physical tendencies.

Results of seasonal simulations have been shown to be free of systematic differences linked to the spatial interpolation and to the coarser resolution of both the inputs to and the outputs from the radiation transfer schemes. When the radiation fluxes and tendencies are considered, averaged over a season, there are differences, but usually much smaller than can be found for a change in cloud optical properties and/or radiation scheme (Morcrette et al., 2001, Morcrette et al., 2007). Furthermore, the new interpolation strategy, by using spatially averaged quantities as inputs, is a better framework to tackle the spurious behaviour sometimes generated by the previously operational sampling scheme, when heavy precipitation could appear over islands due to a mismatch between the atmospheric profiles feeling the orography and surface forcing representative of ocean conditions.

In high-resolution $T_L 799 L91$ ten-day forecasts, the differences in the objective scores are also very small and only appear in the last two days of the ten-day forecasts. Impact on analyses and on two-metre temperature around coastline or orographic features is small and only reaches 1 K for the coarsest spatial interpolation used.

Operationally, the ECMWF IFS is used for different purposes with a variety of resolution. Up to October 2003, the configuration with a sampling down to 1 point out of 4 in the longitudinal direction was used for all applications: high-resolution ten-day forecasts at T_L511, ensembles of T_L255 ten-day forecasts for the Ensemble Prediction System, and seasonal forecasts at T_L95. From October 2003 to May 2007, for both the high-resolution and the ensembles of ten-day forecasts, the radiation grid was coarser than the grid for the rest of model by a factor of two. This and the increase in vertical resolution and associated decrease in the length of the time step allowed for more frequent radiation computations (every one hour) to improve the interactions between radiation, convection and cloud processes.

With the new and more computer intensive McRad package, the versatile interface between radiation and the rest of the model is now used with various radiation resolutions depending on the application. For the high resolution deterministic model run at $T_L799L91$, the radiation grid has been reduced to R319 without any detrimental impact on the quality of the forecasts as judged from the objective scores and comparisons of surface parameters with observations.

For the EPS run at $T_L399L62$, given the approach used to deal with the physical tendencies, a more drastic reduction on the resolution of the radiation grid has been shown to have very limited impact of the quality of the forecasts.

At the low resolution used for testing the impact of model developments on the model climate, it was shown that running the model at T_L159 with a R159 radiation grid does not bring obvious improvements when the sea surface temperature is specified, and that a R63 radiation grid is adequate for such sensitivity studies.

At the same low resolution, in seasonal forecasts with a coupled ocean, the signal brought by the different radiation grids is far from systematic, and it would be necessary to run a much more extended set of simulations to get statistical significance. However, given that the seasonal forecasts are also run as an ensemble from perturbed initial conditions, the R63 radiation grid for the T_L159 model is a good trade-off between accuracy and efficiency.

Appendix

At ECMWF, the interface for radiation computations in the Integrated Forecasting System (IFS) has evolved over the years to accommodate changes in computer architecture.

1/ Prior to the mid-90's ECMWF's computer systems were CRAY vector systems having up to 16 processors accessing a single shared memory. The parallelisation strategy for grid-point computations (i.e., physics including radiation, and dynamics) on these systems was implemented by assigning full latitudes dynamically to processors via a macro-tasking interface. For the radiation calculations, inputs were interpolated from the regular model grid to the radiation grid by a Fast Fourier Transform and likewise outputs from the radiation grid to model grid. In this configuration, the full radiation computations, done every three hours were carried out for all latitude lines with a horizontal resolution four times lower in the longitudinal direction. On this reduced radiation grid, a shortwave (SW) transmissivity was computed at the layer interface by dividing the net SW flux by μ, the cosine of the solar zenith angle at the mid-point of the time interval between two full radiation calculations. These full radiation quantities were then interpolated back using an inverse FFT to the normal physical grid. The net longwave fluxes were kept fixed between two full radiation time steps whereas the net SW fluxes were evaluated at every time step. For every time step within the period between two full radiation computations, the net SW fluxes were obtained by multiplying the SW transmissivity by μ relevant for the time step and grid point. This approximate treatment therefore made the radiation fields interact with cloudiness only every three hours, and further introduced spatial smoothing of the cloud-radiation interactions.

2/ From September 1991, the ECMWF model started to use a reduced horizontal grid for all its computations, keeping roughly the same grid size (in km) when going from Equator to poles (Hortal and Simmons, 1991). The change in distributed memory vector systems (Fujitsu VPP700/VPP5000) presented a problem for the above scheme on the reduced horizontal grid as a 2-dimensional partitioning of grid point space required on these systems meant that only a subset of points on each latitude were directly accessible. Furthermore, the message passing to gather full latitudes for the above FFT's was considered an unacceptable overhead. The solution to these problems was found by a combination of separating the radiation calculations from the physics call tree and providing new interpolation options for radiation input and output. On input, model fields required by the radiation package were sampled on each latitude with one point out of four being selected in sub-tropical and tropical areas. To accommodate the reduced model grid this frequency of one in four reduced gradually to every point in polar areas. This latter requirement resulted in a substantial load imbalance for radiation calculations, which was resolved by message passing to distribute radiation points evenly (Dent and Mozdzynski, 1996). On output, lagrangian cubic interpolation was used which required some further message passing (albeit nearest neighbour). On the whole this scheme has worked efficiently on both vector systems with less than 100 processors and scalar systems with about 1000 processors. The only real drawback was the complexity of the message passing, which was a direct result of the use of a non-standard grid for radiation calculations (i.e, the sampled grid). Some concern was also raised with regard to the sampling approach, in particular the issue that sampling was only implemented East-West and not North-South.

3/ The new (October 2003) interface for radiation computations was developed to address some deficiencies of the scheme described above, by use of a standard IFS model grid for radiation calculations. With this interface, radiation calculations are performed on a grid with a lower coarser resolution than the current model grid. Interpolation between model and radiation grids are performed using interfaces existing within the IFS libraries and as a result this reduces future code maintenance.

By using such a standard grid for radiation calculations, there is no longer a load balance issue as each processor is given an equal number of grid points for both model and radiation grids. Interpolation options provided include spectral transform, four-point bi-linear, and 12-point bi-dimensional interpolation. It is to be noted that the spectral transform option is provided for debugging purposes only - in the ECMWF spectral model it was the most straightforward option to implement and it simplified the development and testing of the other options. It is also the most expensive in respect of CPU time and memory use. The technical aspects of the transformation package including these last two interpolations are described in Hamrud (2001).

REFERENCES

Buizza, R., M.J. Miller and T.N. Palmer, 1999: Stochastic representation of model uncertainties in the ECMWF Ensemble Prediction System. *Quart. J. Roy. Meteor. Soc.*, **125**, 2887–2908.

Buizza, R., J.-R. Bidlot, M. Wedi, M. Fuentes, M. Hamrud, G. Holt and F. Vitart, 2007: The new ECMWF VAREPS (Variable Resolution Ensemble Prediction System). *Quart. J. Roy. Meteor. Soc.*, **133**, 681-695.

Chevallier, F., J.-J. Morcrette, F. Cheruy, and N.A. Scott, 2000: Use of a neural-network-based longwave radiative transfer scheme in the ECMWF atmospheric model. *Quart. J. Roy. Meteor. Soc.*, **126**, 761-776.

Da Silva, A.M., and S. Levitus, 1994: *Atlas of surface marine data. Vol. I: Algorithms and procedures.* National Oceanic and Atmospheric Administration. NOAA Atlas NESDIS **6**, Washington DC, USA, 83 pp.

Dent, D., and G. Mozdzynski, 1996: ECMWF Operational Forecasting on a Distributed Memory Platform. *Proceedings, 7th ECMWF Workshop on the Use of Parallel Processors in Meteorology*, World Scientific, 36-51.

Hamrud, M., 2001: New Transform Library, ECMWF Research Department Memorandum R48/MH/4, 9pp.

Hortal, M., and A.J. Simmons, 1991: Use of reduced Gaussian grids in spectral models. *Mon. Wea. Rev.*, **119**, 1057-1074.

Janisková, M., J.-F. Mahfouf, J.-J. Morcrette, and F. Chevallier, 2002: Linearized radiation and cloud schemes in the ECMWF model: Development and evaluation. *Quart. J. Roy. Meteor. Soc.*, **128**, 1505-1527.

Majewskie, D., D. Liermann, P. Prohl, B. Ritter, M. Buchold, T. Hanisch, G. Paul, and W. Wergen, 2002: The operational global icosahedral-hexagonal grid point model GME: Description and high-resolution tests. *Mon. Wea. Rev.*, **130**, 319-338.

Morcrette, J.-J., 2000: On the effects of the temporal and spatial sampling of radiation fields on the ECMWF forecasts and analyses. *Mon. Wea. Rev.*, **128**, 876-887.

Morcrette, J.-J., H.W. Barker, J.N.S. Cole, M.J. Iacono, and R. Pincus, 2007: Impact of a new radiation package, McRad, in the ECMWF Integrated Forecasting System. *Mon. Wea. Rev.*, submitted.

Uppala, S.M., et al. 2005: The ERA-40 re-analysis. *Quart. J. R. Meteor. Soc.*, **131**, 2961-3012.

Vialard, J., F. Vitart, M.A. Balsameda, T.N. Stockdale and D.L.T. Anderson, 2005: An ensemble-generation method for seasonal forecasting with an ocean-atmosphere coupled model. *Mon. Wea. Rev.*, **133**, 441-453.

List of Figures

FIG. 1. The r.m.s. error (top panels) and mean error (bottom panels) of the temperature at 850 hPa (left panels) and 200 hPa (right panels) in the Tropics (20^oN - 20^oS) for McRad 10-day forecasts at $T_L399L62$, started every 96 hours from 2006021212 to 2007020512, and using the six different radiation grids from $R255$ to $R31$ given in Table 1.
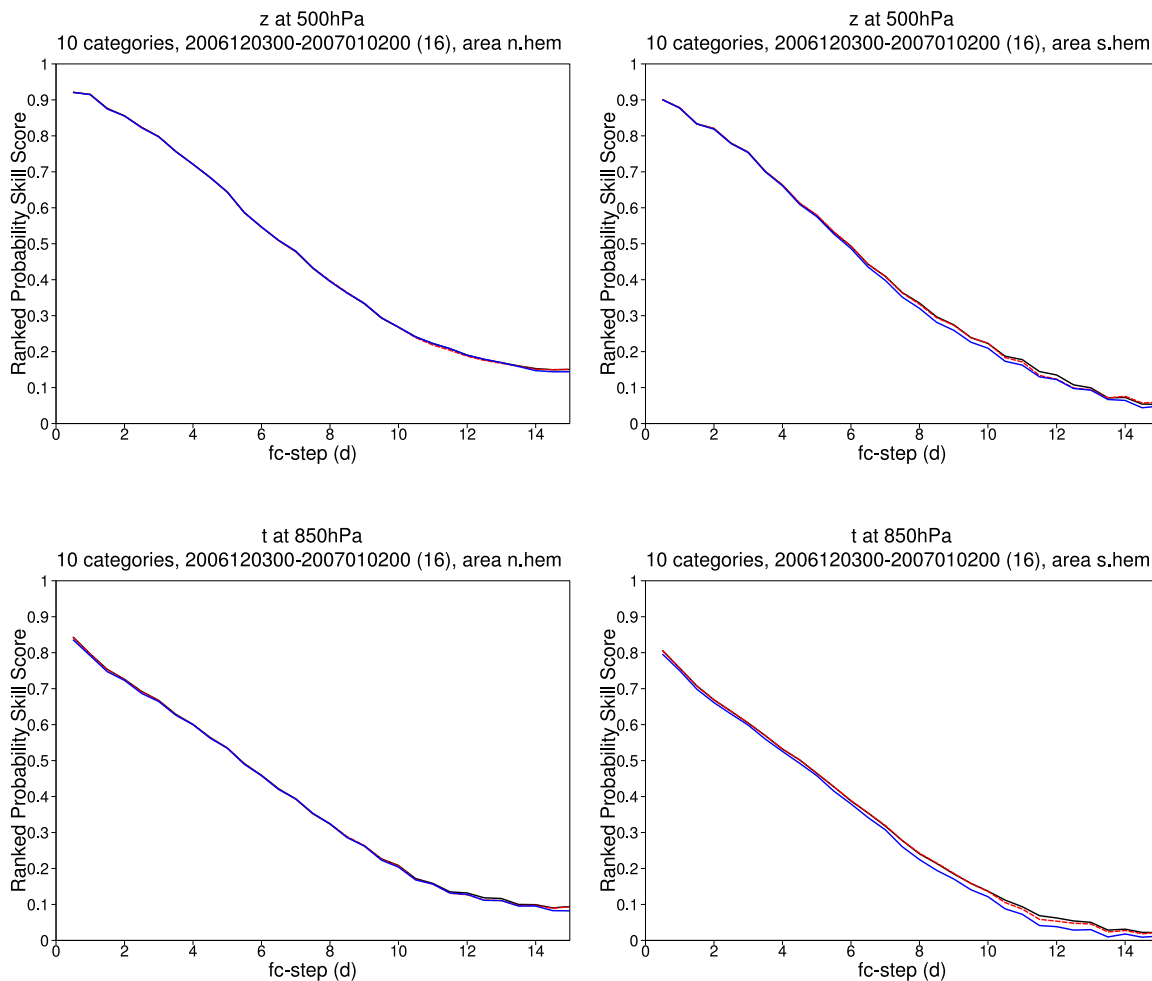
FIG. 2. The ranked probability skill score for the geopotential at 500 hPa (upper panels) and the temperature at 850 hPa (lower panels) for the Northern (left column) and Southern (right column) hemispheres for the 32R2 EPS, with three sets of radiation grids: Black curve is for R159/R95, red for R95/R63, blue for R47/31. Results are for 16 forecasts started every 48 hours from 20061203 00UTC.
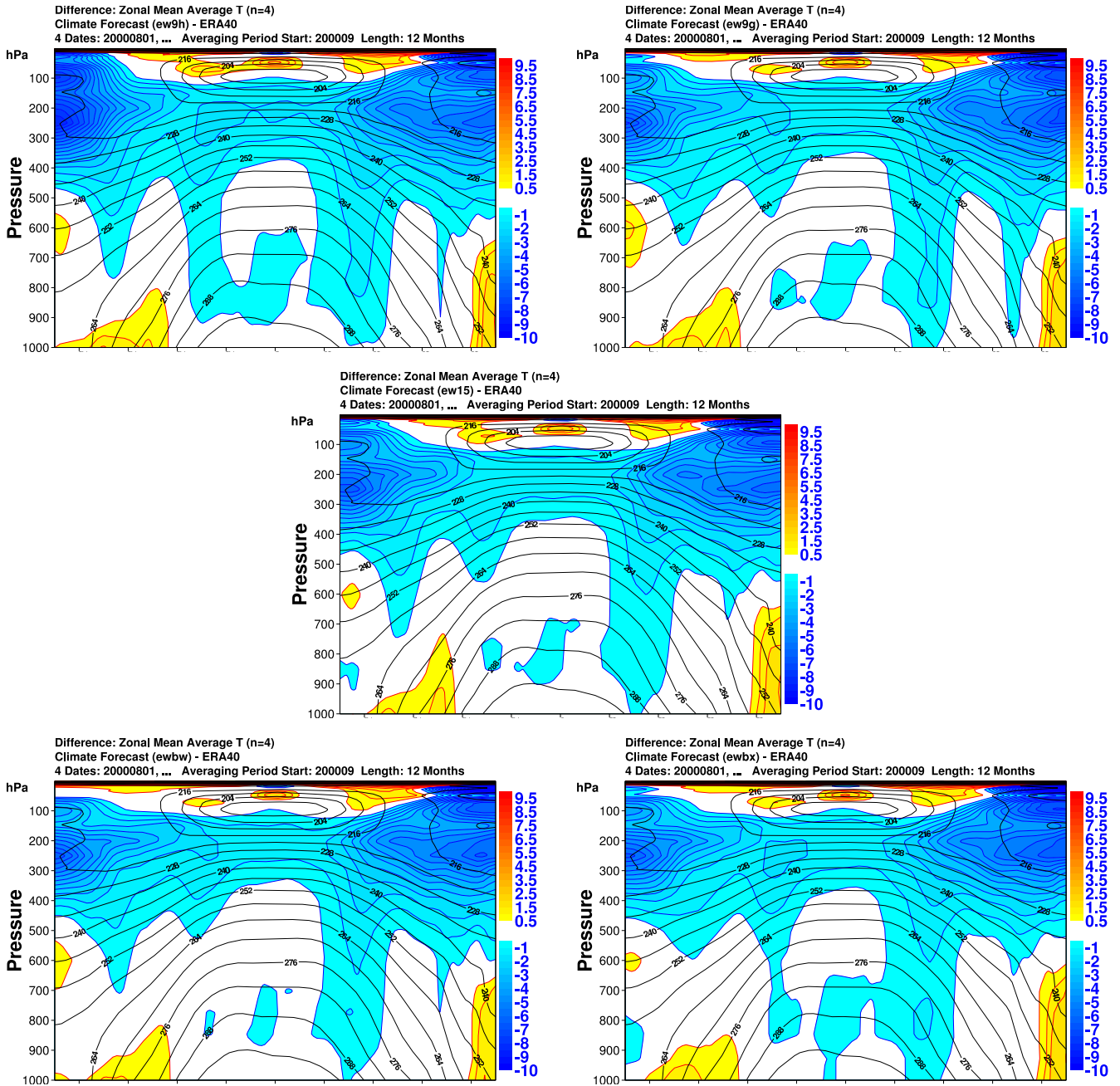
FIG. 3. The zonal mean difference between the annually averaged temperature and the corresponding ERA40 analysis (in K). All models have a $T_L 159$ resolution for dynamics and are run with a specified sea surface temperature. Resolution for radiation is respectively R159 (top left), R95 (top right), R63 (middle), R47 (bottom left) and R31 (bottom right).
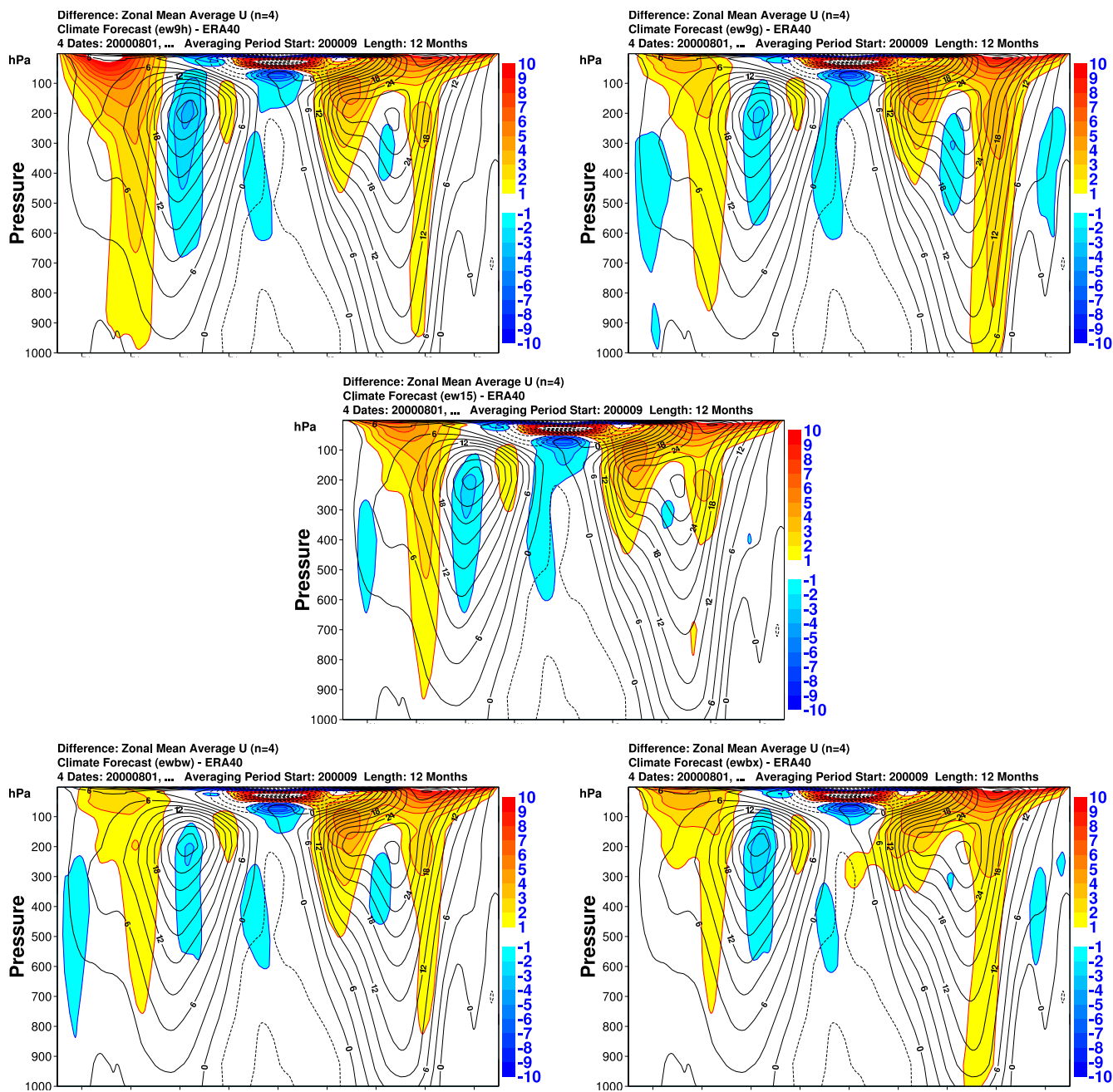
FIG. 4. As in Fig. 3, but for the zonal mean difference between the annually averaged zonal wind and the corresponding ERA40 analysis (in ms^{-1}).
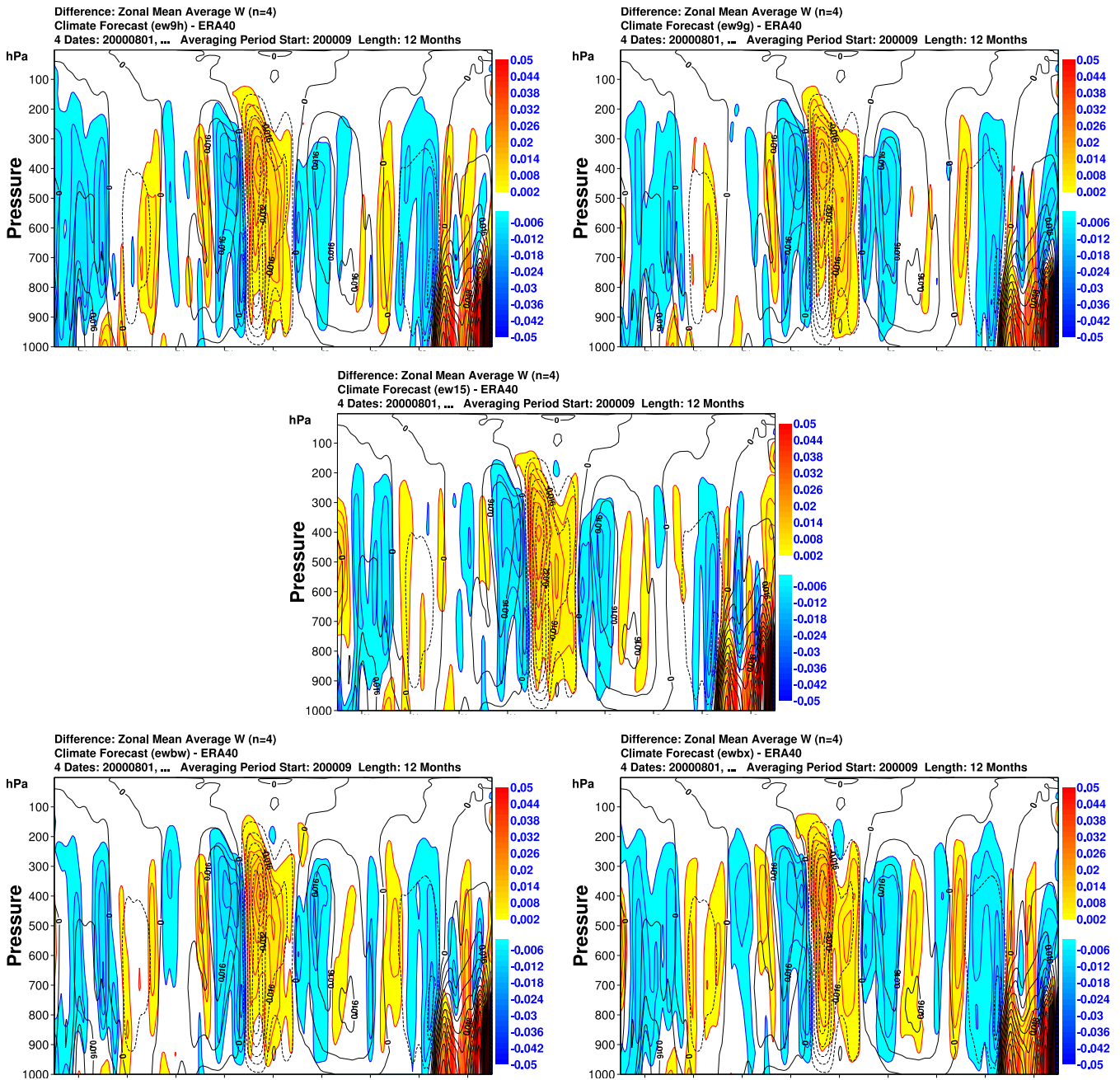
FIG. 5. As in Fig. 3, but for the zonal mean difference between the annually averaged vertical velocity and the corresponding ERA40 analysis (in *Pa s^{-1}*).
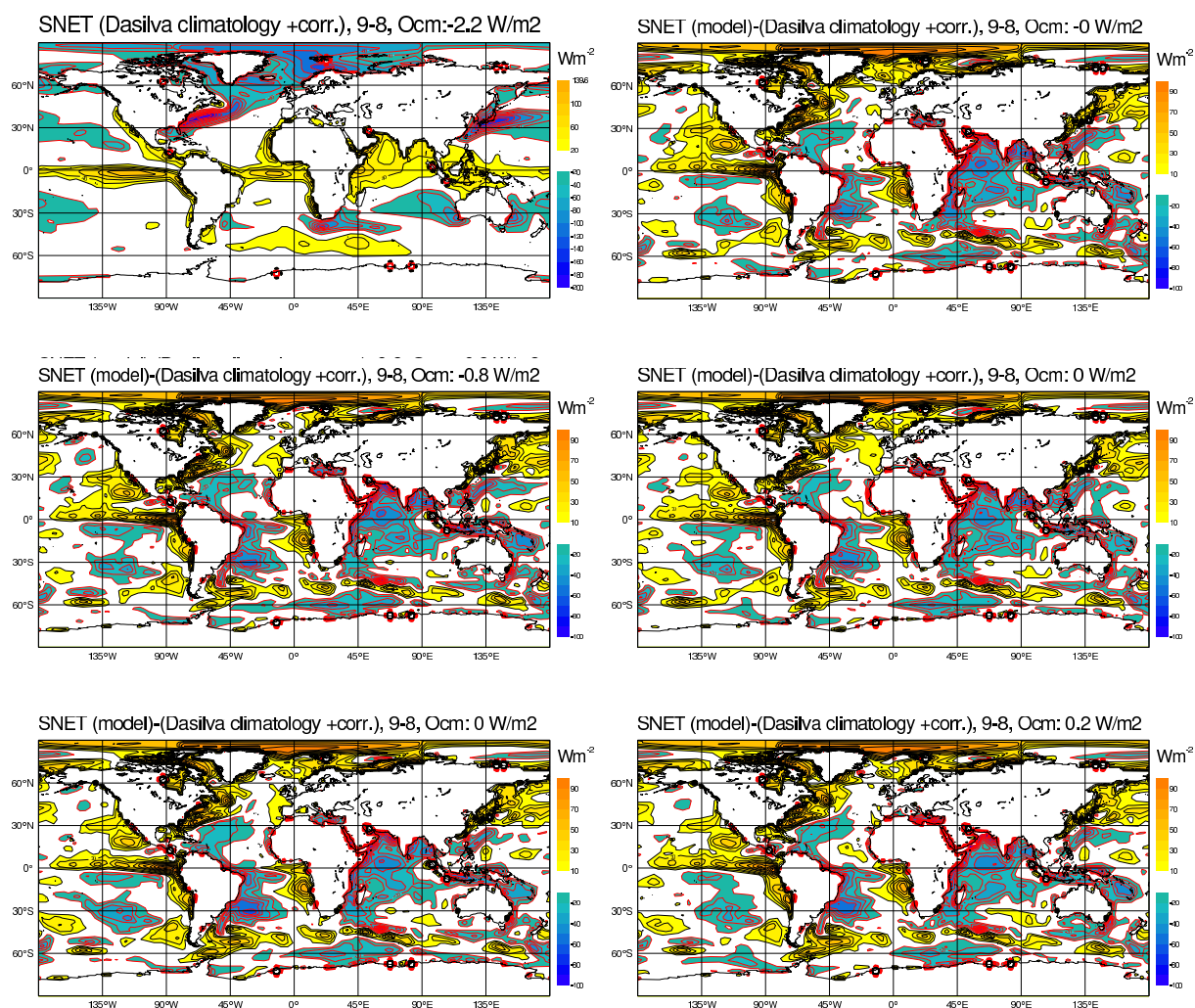
FIG. 6. The annual mean net energy flux at the surface (in Wm^{-2}). Top left panel is the Da Silva-Levitus climatology. The other panels are the difference between the model with specified SSTs and the climatology, for the model with a R159 (middle left), R95 (bottom left), R63 (top right), R47 (middle right) and R31 radiation grid, respectively.
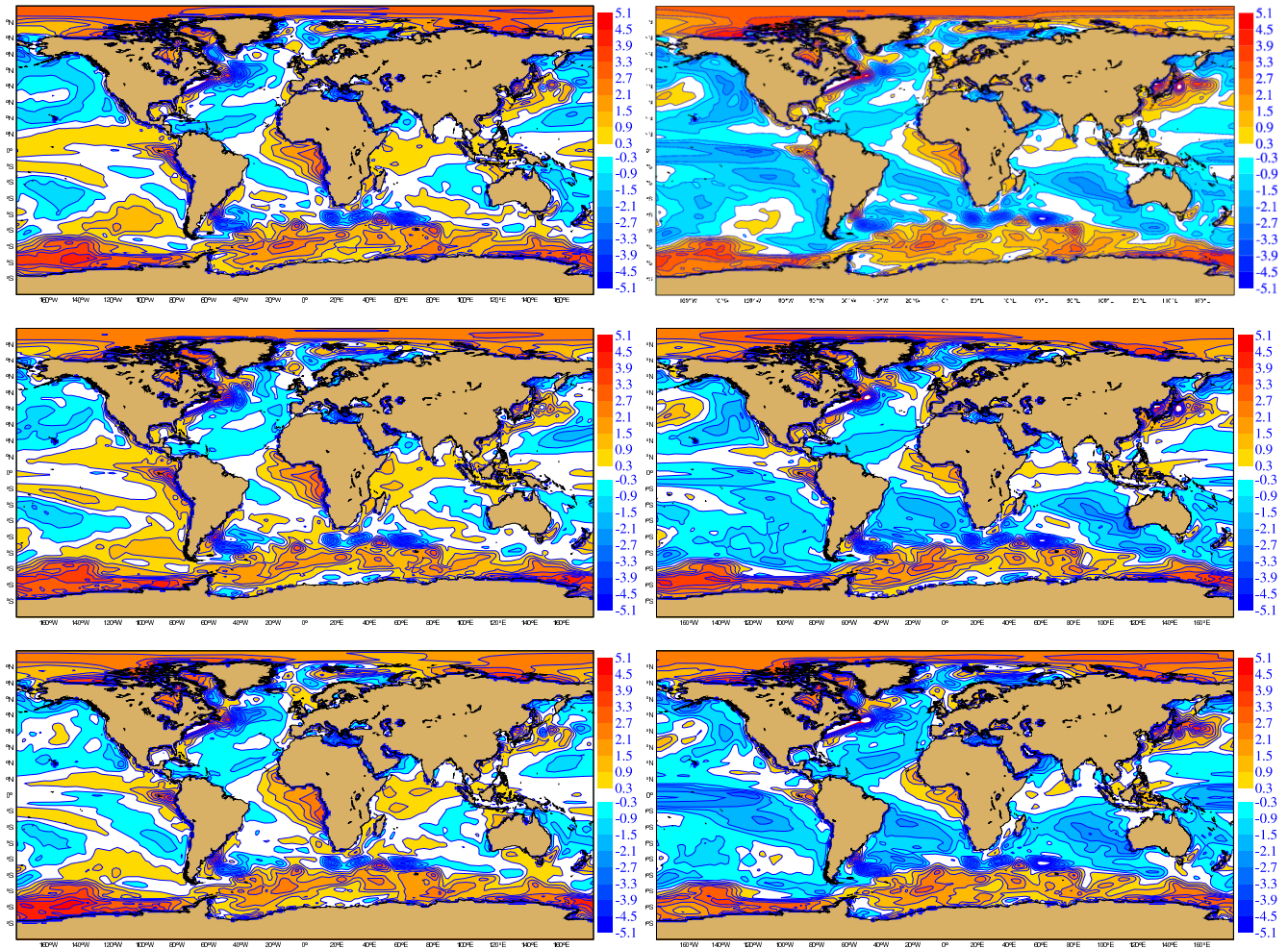
FIG. 7. Comparison of annual mean sea surface temperature (SST) produced by the $T_L 159$ model with different radiation grids, for year 1 (left panels) and year 2 (right panels). Differences are with ERA40. Top panels are for $R159$, middle panels for $R63$, and lower panels for $R31$. All values in K.